How to cite: *Angew. Chem. Int. Ed.* **2024**, *63*, e202403313
doi.org/10.1002/anie.202403313

Chiral Polymers | Hot Paper

Size Control of Chiral Nanospheres Obtained via Nanoprecipitation of Helical Poly(phenylacetylene)s in the Absence of Surfactants

*Manuel Núñez-Martínez[+], Manuel Fernández-Míguez[+], Emilio Quiñoá, and Félix Freire**

Abstract: Nanostructuration of dynamic helical polymers such as poly(phenylacetylene)s (PPAs) depends on the secondary structure adopted by the polymer and the functional group used to connect the chiral pendant to the PPA backbone. Thus, while PPAs with dynamic and flexible scaffolds (*para*- and *meta*-substituted, $\omega_1 < 165°$) generate by nanoprecipitation low polydisperse nanospheres with controllable size at different acetone/water mixtures, those with a quasi-static behavior and the presence of an extended, almost planar structure (*ortho*-substituted, $\omega_1 > 165°$), aggregate into a mixture of spherical and oval nanostructures whose size is not controlled. Photostability studies show that poly(phenylacetylene) particles are more stable to light irradiation than when dissolved macromolecularly. Moreover, the photostability of the particle depends on the secondary structure of the PPA and its screw sense excess. This fact, in combination with the encapsulation ability of these polymer particles, allows the creation of light stimuli-responsive nanocarriers, whose cargo can be delivered by light irradiation.

Introduction

Polymer-based chiral nanostructures have recently been studied by the scientific community due to the combination of chirality and nanotechnology, allowing the creation of new materials with interesting applications in catalysis, photonics, sensors, drug-delivery or bioimaging.[1–9] From these materials it is possible to create micelles, nanospheres or capsules, where the size and morphology control is a very important issue due to the properties associated to these parameters such as the surface area, diffusibility and mobility. Dynamic helical polymers[10–36] show interesting stimuli-responsive properties[37] that allow controlling their helical sense and/or elongation. This fact makes these polymers attractive to be applied at the nanoscale level, where *P*/*M* dynamic chiral polymer particles can find potential applications in fields such as asymmetric catalyst,[38–39] CPL light-emissive materials,[40–42] enantioseparation,[43] stimuli-responsive particles,[44] crystallization,[45] chiral resolution,[46] drug delivery[47] and so on. PPAs stand out within this family of polymers due to their versatility. The robustness of the polymerization reaction with a Rh(I) catalyst permits to synthetize polymers from monomers containing a large variety of functional groups. As a result, in these polymers it is possible to analyze the parameters that affect their secondary structure and folding degree, such as the aromatic substitution pattern, the use of spacers between the backbone and the chiral center, or even the functional group used to connect the PPA backbone with the pendant group. In a pioneering work, Deng and coworkers explored the self-assembly of poly(acetylene)s (PAs) into chiral nanospheres via nanoprecipitation.[48–50] However, the relationship between the secondary structure of a PA and its aggregation capacity was not explored in these studies. In the literature, it is found that the nanostructuration of helical polymer-metal complexes (HPMCs) occurs using PPAs as helical polymers and different metal ions as crosslinking agents.[51–56] From these studies, it was found that is possible to tune the chirality, the size, and the morphology (nanospheres, nanotubes or toroids) of the aggregates by varying the polymer/metal ion ratio and the solvent conditions. However, in HPMCs, the metal ion alters the secondary structure and the stiffness of the polymer, making it not possible to establish a secondary structure/nanostructure relationship.[55]

In this work, we aim to determine the macromolecular helical structure/nanostructure relationship using a nanoprecipitation approach for a library of PPAs with different secondary structure (elongation and stiffness) and functional groups used to link the PPA backbone to the chiral pendant group (anilide/benzamide) (Scheme 1).

Results and Discussion

PPA elongation degree and polymer particle control. To perform these studies, a library of nine chiral PPAs with

[*] Dr. M. Núñez-Martínez,[+] M. Fernández-Míguez,[+] Prof. E. Quiñoá, Prof. F. Freire
Centro Singular de Investigación en Química Biolóxica e Materiais Moleculares and Departamento de Química Orgánica, Universidade de Santiago de Compostela, E-15782 Santiago de Compostela, Spain
E-mail: felix.freire@usc.es

[+] These authors contributed equally to this work

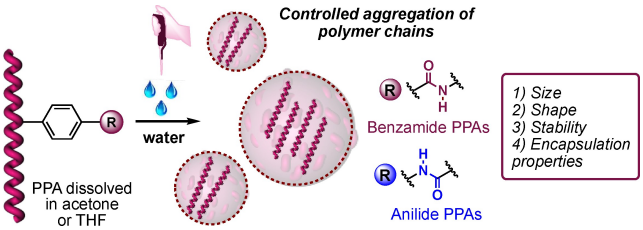

Scheme 1. Illustration of the nanoprecipitation protocol to prepare chiral nanospheres.

well-known secondary structure and different helical scaffold was selected as follows: 1) *Cis-cisoidal* PPAs ($\omega_1 < 90°$). Two PPAs containing anilide connectors (poly-(*R*)-**1** and poly-(*R*)-**2**; Figure 1) where chosen due to their ability to generate compact *cis-cisoidal* structures—dihedral angles between conjugated double bonds $\omega_1 < 90°$—.[25,57] 2) *Cis-transoidal* PPAs ($90° < \omega_1 < 160°$). Four PPAs containing a benzamide connector (poly-(*S*)-**3**, poly-(*S*)-**4**, poly-(*S*)-**5**, poly-(*S*)-**6**; Figure 1) were selected because they generate more extended *cis-transoidal* structures ($90° < \omega_1 < 160°$).[53] In all cases, the selected PPAs present dynamic helical scaffolds, whose helical sense can be amplified or inverted by the action of external stimuli (e.g., metal ions).[51,53,55]

Poly-(**1**–**6**) were prepared according to literature using rhodium norbornadiene chloride dimer, $[Rh(nbd)Cl]_2$, as catalyst (see Supporting Information for experimental and characterization details). Next, poly-(**1**–**6**) were aggregated using a nanoprecipitation protocol, which consists of dissolving the polymers in acetone or THF (good solvents), followed by the addition of water (poor solvent) until reaching a $V_{acetone/THF}/V_{water}$ ratio of 100/900, 300/700 and 500/500 (μL/μL) (final volume: 1 mL, 0.3 mg/mL). Dynamic light scattering (DLS) studies showed, in all cases, the presence of low polydisperse chiral polymer particles [light scattering polydispersity index (PDI) < 0.2], whose size can be tuned by varying the water content in the solvent mixture (Table 1 for acetone/water mixtures and Supporting Information for THF/water mixtures). For instance, small polymer particles (diameter < 100 nm) are obtained for poly-(**1**–**6**) when the dispersions are prepared in a 100/900 (μL/μL) $V_{acetone}/V_{water}$ ratio, while the particle size grows progressively by decreasing the water content in the poly-(**1**–**6**) acetone/water mixtures (Table 1). For example, poly-(*R*)-**1** generates 90, 230 and 526 nm polymer particles in acetone/water mixtures at 100/900, 300/700 and 500/500 (μL/μL) $V_{acetone}/V_{water}$ ratio respectively, while poly-(*S*)-**6** generate 70, 129 and 413 nm polymer particles under the same conditions. In the case of using THF/water mixtures to prepare the polymer particles, the size of the aggregates are larger than those observed when acetone is used as organic solvent. However, the pattern of size variation found in both organic solvent/water mixtures follow the same trend, with an increase in particle size as the water content decreases in the solvent mixture (see Table 1 and SI). Therefore, nanoprecipitation allows controlling the particle size of anilide and benzamide PPAs in the absence of surfactants.

Next, the morphology of the polymer particles was studied by atomic force microscopy (AFM) and surface electron microscopy (SEM). Thus, 10 μL of poly-(*R*)-**1**, poly-(*R*)-**2**, poly-(*S*)-**3**, poly-(*S*)-**4**, and poly-(*S*)-**6** dispersions prepared in a 300/700 (μL/μL) $V_{acetone}/V_{water}$ ratio were drop-casted onto different silicon wafer substrates and submitted to AFM (poly-(*R*)-**1** and poly-(*S*)-**6**) and SEM (poly-(*R*)-**1**, poly-(*R*)-**2**, poly-(*S*)-**3**, and poly-(*S*)-**4**) studies. Interestingly, while high-resolution AFM images show the presence of spherical aggregates whose size agrees with the data obtained from DLS experiments (size and PDI), i.e., 200 nm for poly-(*R*)-**1** and 140 nm for poly-

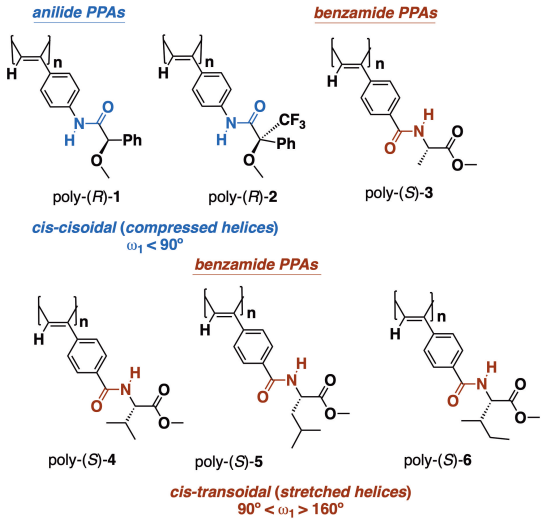

Figure 1. Molecular structures of PPAs selected for nanoprecipitation studies.

Table 1: DLS data for poly-(**1**–**6**) nanospheres obtained in different acetone/water mixtures. [polymer] = 0.3 mg/mL.

PPAs (size, PDI[a])	acetone/water [v (μL)/v(μL)]		
Poly-(*R*)-**1**	100/900	300/700	500/500
Size/nm	90	230	526
PDI	0.198	0.101	0.151
Poly-(*R*)-**2**	100/900	300/700	500/500
Size/nm	55	385	422
PDI	0.122	0.014	0.006
Poly-(*S*)-**3**	100/900	300/700	500/500
Size/nm	56	84	230
PDI	0.095	0.098	0.086
Poly-(*S*)-**4**	100/900	300/700	500/500
Size/nm	90	173	425
PDI	0.083	0.145	0.067
Poly-(*S*)-**5**	100/900	300/700	500/500
Size/nm	68	132	312
PDI	0.130	0.125	0.031
Poly-(*S*)-**6**	100/900	300/700	500/500
Size/nm	70	129	413
PDI	0.139	0.140	0.021

[a]PDI (light scattering polydispersity index)

(*S*)-**6** at 300/700 (μL/μL) $V_{acetone}/V_{water}$ (Figure 2), surface electron microscopy (SEM) corroborates the presence of spherical particles although their size depends on the anilide/benzamide functional group used to connect the pendant group to the poly(phenylacetylene) backbone. Thus, in the case of anilide-PPAs—poly-(*R*)-**1** and poly-(*R*)-**2**—, the sizes of the nanospheres obtained from SEM studies (230 nm for poly-(*R*)-**1**; 264 for poly-(*R*)-**2**, Figure 3a) are similar to those obtained from DLS (160 nm for poly-(*R*)-**1**; 385 nm for poly-(*R*)-**2**, Table 1) and AFM studies (140 nm for poly-(*R*)-**1**, Figure 2a). However, in the case of benzamide-PPAs—poly-(*S*)-**3**, and poly-(*S*)-**4**—, the sizes of the chiral nanospheres are dramatically reduced when the dispersed polymer particles are prepared in acetone/water mixture and visualized by SEM — i.e., nanospheres from poly-(*S*)-(**3**–**4**) (0.3 mg/mL acetone) dispersed in 300/700 (μL/μL) acetone/water mixtures; DLS: poly-(*S*)-**3** = 93 nm, poly-(*S*)-**4** = 173 nm; SEM images: poly-(*S*)-**3** = 61 nm, poly-(*S*)-**4** = 62 nm—(Figure 3b).

ECD studies were also carried out for the dispersions of poly-(*R*)-**1**, poly-(*R*)-**2**, poly-(*S*)-**3**, and poly-(*S*)-**4**, prepared in 300/700 (μL/μL) $V_{acetone}/V_{water}$ ratios (Figure 3 and SI). These studies show ECD spectra with different intensities, indicating the presence of polymer particles with different helical sense excess for PPAs. Thus, the screw sense excess of the polymer does not affect the morphology (size and shape) of the polymer particle (Figure 3). In contrast, the connector used to link the chiral substituent to the phenylacetylene backbone—benzamide or anilide—plays an important role in the nanostructuration of the PPAs. In both cases, an amide bond is used to link the aryl ring of the PPA and the pendant group, although this connection can be made through the N (anilide) or the C (benzamide) atoms of the amide group. This subtle structural difference between anilides and benzamides has a large impact on the acidity of the amide group, with anilides being much more acidic than benzamides.[26] As a result, during the nanostructuration of the PPAs to form nanospheres, the supramolecular interactions between polymer chains and/or polymer fragments are tighter in PPAs bearing anilides than in PPAs possessing benzamides as connectors. In consequence, anilide-PPA nanospheres are stable under high vacuum, which indicates the presence of compact nanostructures, while benzamide-PPA nanospheres shrink in high-vacuum, indicating the presence of less dense and fluffier nanospheres. To demonstrate the anilide/benzamide effect in the nanostructuration of PPAs, oligomer series with different degree of polymerization (DP) of anilide—oligo-(*R*)-**1** and oligo-(*S*)-**2**—and benzamide—oligo-(*S*)-**3**, oligo-(*S*)-**4**, and oligo-(*S*)-**5**—phenylacetylene monomers were prepared following the method previously reported by Maeda and co-workers (Tables S3–S7).[58–61] Nanoprecipitation studies show that in all cases, the addition of water to an acetone or THF solution of the oligomer results in the formation of nanospheres whose size increases as the organic content in the solution mixture increases (see Figure 4a for oligo-(*S*)-**2** (DP = 5 and 9) and

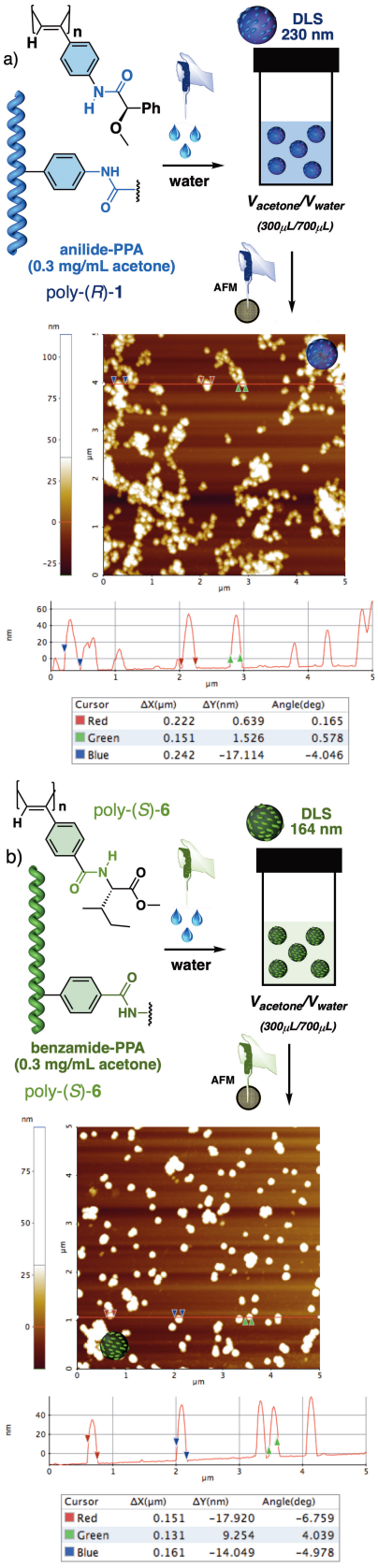

Figure 2. AFM images and height profiles of (a) poly-(*R*)-**1** and (b) poly-(*S*)-**6** nanospheres obtained from nanoprecipitation.

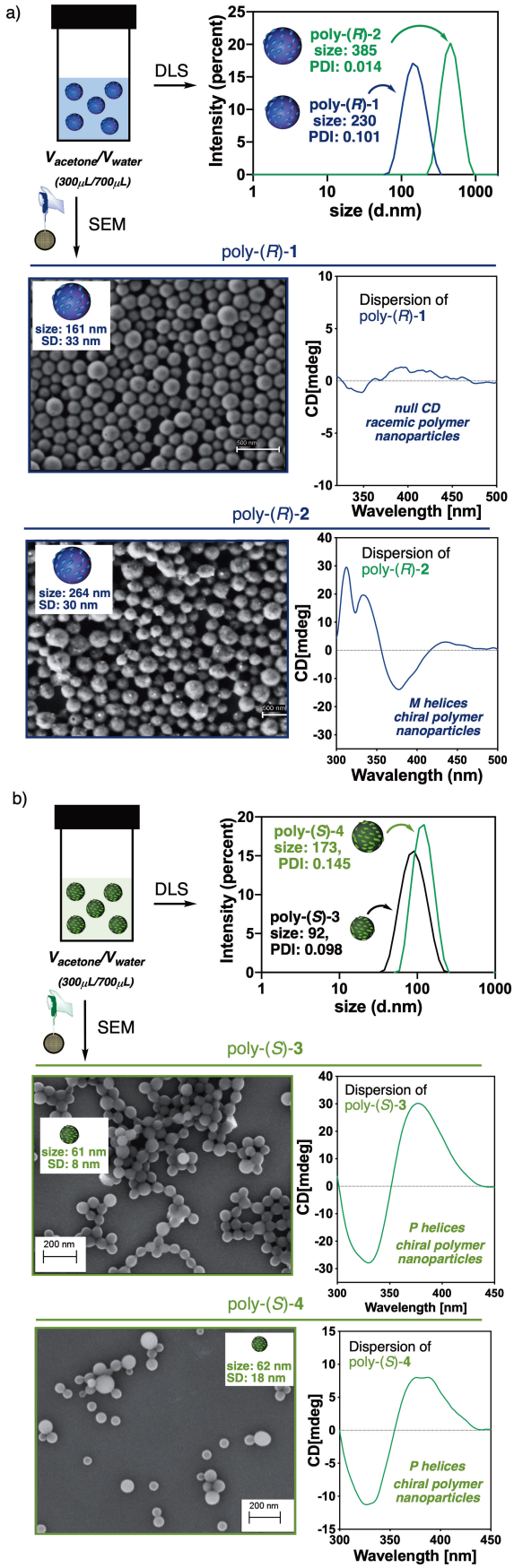

Figure 3. DLS, TEM and ECD studies of (a) anilide- [poly-(*R*)-**1** and poly-(*R*)-**2**] and (b) benzamide- [poly-(*S*)-**3** and poly-(*S*)-**4**]-PPAs.

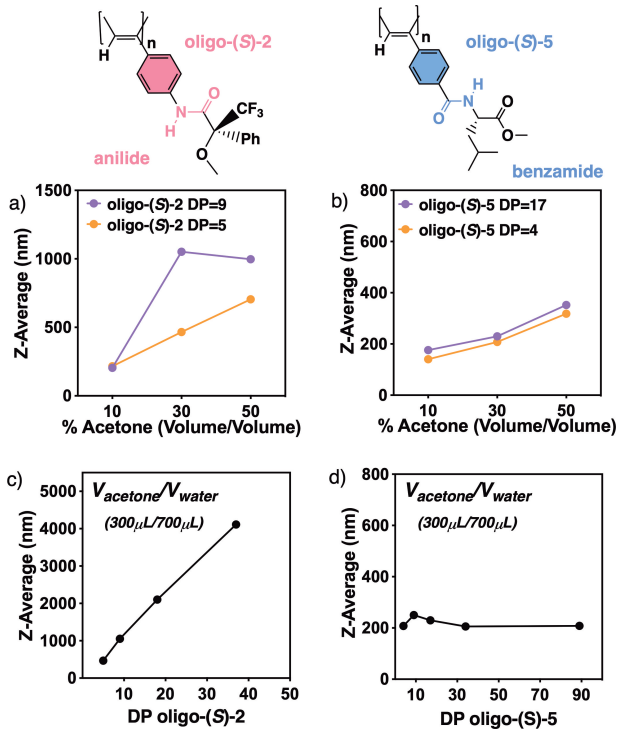

Figure 4. DLS nanoprecipitation studies of (a) anilide—oligo-(*S*)-**2**— and (b) benzamide—oligo-(*S*)-**5**—oligomer series with different DP and at different acetone/water ratios. Variation of the particle size obtained via nanoprecipitation in acetone/water 300/700 ratios for (c) oligo-(*S*)-**2** at DP = 6, 9, 18 and 36 and (d) oligo-(*S*)-**5** at DP = 4, 9, 17, 34 and 89. [oligomer] = 0.3 mg/mL

Figure 4b for oligo-(*S*)-**5** (DP = 4 and 17); see Supporting Information for other DP and oligomers).

However, different aggregation patterns are clearly differentiated from DLS studies for both anilide and benzamide oligomers. Thus, while in the case of anilide oligomers—e.g., oligo-(*S*)-**2** (Figure 4c)—, the particle size obtained from nanoprecipitation studies for a certain organic solvent/water mixture increases as the DP increases in the oligomer series, in the case of benzamide oligomers,—e.g., oligo-(*S*)-**5** (Figure 4d), the particle size is not affected by the DP. Moreover, DLS studies show a larger aggregation tendency in anilide-oligomers than in benzamide-oligomers. Thus, while anilide oligomers can form aggregates from nanometer (200 nm) to micron size (4 μm), benzamide oligomers self-assemble in a range of few hundred nanometers (200–300 nm). Hence, these studies corroborate that small variations in the acidic behavior of the amide group used to connect the pendant and the PPA backbone can have a large impact on the intra- and intermolecular hydrogen bonding interactions and, therefore, on the aggregation pattern of helical polymers such as PPAs.

To complete this work and determine how the secondary structure of PPAs affects their nanostructuration ability, other polymers adopting more stretched scaffolds ($\omega_1 > 160°$) were selected from the literature. The aromatic substitution pattern in PPAs (*para-*, *meta-*,

ortho- series) is known to affect the stretching, stiffness and dynamic behavior of the macromolecular helical structure they adopt.[25] Thus, while *para*-substituted PPAs normally adopt the most compressed helix of the polymer series, their *meta*- and *ortho*-counterparts adopt more elongated scaffolds, being almost planar ($\omega_1 > 170°$) for the *ortho*-substituted ones.

3) *Cis-transoidal* PPAs ($\omega_1 > 160°$). To complete these studies, two *meta*-substituted [*m*-poly-(*R*)-**7** and *m*-poly-(*S*)-**8**] and one *ortho*-substituted [*o*-poly-(*R*)-**9**] PPAs were chosen as model compounds of PPAs with highly stretched polyene backbones (Figures 5a–b). Thus, poly-(**7**–**9**) were prepared from the appropriate phenylacetylene monomers using a Rh(I) catalyst (see Supporting Information for experimental and characterization details). Next, the corresponding chiral polymer particles were prepared by dissolving poly-(**7**–**9**) in acetone and THF (0.3 mg), followed by the addition of water until reaching $V_{acetone/THF}/V_{water}$ ratios of 100/900, 300/700 and 500/500 (μL/μL)—final volume: 1 mL—. Interestingly, in the case of *meta*-substituted PPAs, DLS studies for the acetone/water mixtures revealed the formation of low polydisperse nanospheres (PDI < 0.2), whose size can be tuned by controlling the amount of water (Table 2 for dispersions in acetone/water and Supporting Information for THF/water), while in the case of the *ortho*-substituted PPA (poly-**9**), the aggregate cannot be controlled. The poor nanostructuration ability of *ortho*-substituted PPAs can be explained by considering the presence of an almost planar helical scaffold, which exposes the hydrophobic poly(phenylacetylene) backbone to the solvent. In the case of *para*- and *meta*-substituted PPAs, the presence of more twisted helical structures places the pendant groups around the hydrophobic poly(phenylacetylene) backbone. As a result, poly(phenylacetylene)/water interactions are reduced, allowing PPA aggregation to be controlled.

SEM studies for anilide and benzamide *meta*-substituted PPAs show analogous patterns as those observed in their *para*-substituted counterparts. *m*-Poly-(*R*)-**7** (anilide-PPA, $c = 0.3$ mg/mL) in 100/900 (μL/μL) acetone/water produces a dispersion of nanospheres with a diameter of 78 nm (DLS), and a similar size is observed under high vacuum with a diameter of 80 nm (SEM) (Figure 5c). On the other hand, *m*-poly-(*S*)-**8** (benzamide PPA, $c = 0.3$ mg/mL) in 500/500 (μL/μL) acetone/water generates a dispersion of nanospheres with a diameter of 100 nm (DLS), while their size differs under high vacuum with a diameter of 50 nm (SEM) (Table 2 and Figure 5d).

Therefore, the different acidic behavior of the anilide and benzamide groups produces again a variation in the density of the polymer particles, being denser the anilide-PPA particles, while the benzamide PPA particles are fluffier.

Finally, SEM studies for a dispersion of an *ortho*-substituted PPA (*o*-poly-(*R*)-**9**) reveal the presence of nanostructures with different morphology (spheres, ovals, sticks). In this case, the high hydrophobicity of a stretched and stiff helix causes assembly to occur in different longitudinal structures (Figure 5e).

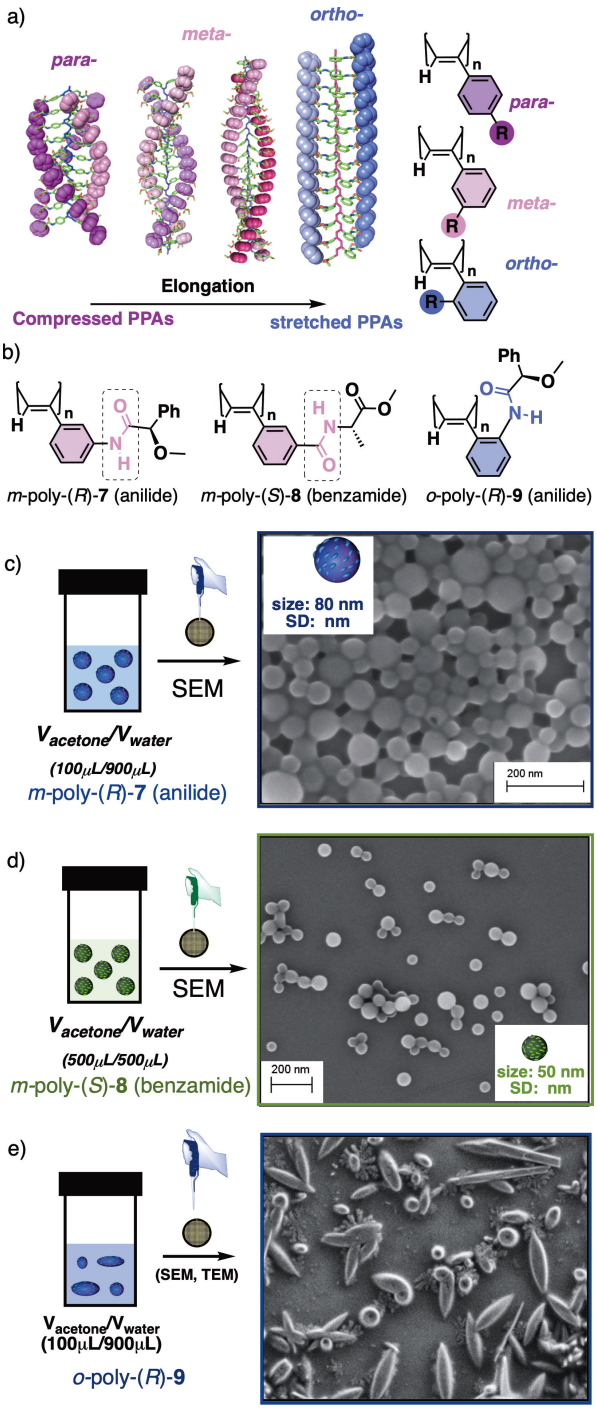

Figure 5. a) Schematic illustration of the elongation effects within *para*-, *meta*- and *ortho*-substituted PPA series. b) Chemical structure of *meta*- and *ortho*-PPAs selected for these studies. DLS, TEM and ECD studies for *meta*-substituted (c) anilide- [*m*-poly-(*R*)-**7** and (d) benzamide- [*m*-poly-(*S*)-**8**] PPAs. e) SEM studies for an *ortho*-substituted PPA (*o*-poly-(*S*)-**9**).

Polymer particle time-dependent and thermal stability studies. Time dependent DLS studies were carried out to determine the stability of the chiral polymer particles obtained from anilide poly-(*R*)-**1** and benzamide poly-(*S*)-**5** using this green chemistry protocol, which does not

Table 2: DLS data for nanospheres of poly-(**7**–**8**) obtained in acetone/water mixtures. [polymer] = 0.3 mg/mL.

PPAs (size, PDI)	acetone/water [v (μL)/v (μL)]		
m-Poly-(*R*)-**7**	100/900	300/700	500/500
Size/nm	78	101	141
PDI	0.170	0.126	0.116
m-Poly-(*S*)-**8**	100/900	300/700	500/500
Size/nm	41	66	100
PDI	0.136	0.093	0.088

require the presence of any surfactant (0.3 mg/mL of dispersed PPA). These studies indicate that polymer particles remain well dispersed in an acetone/water mixture for up to 100 h, a good value considering that no stabilizing agents were added to the dispersed particles (Figure 6a for poly-(*R*)-**1** and 6b for poly-(*S*)-**5**. Furthermore, the stability of the nanospheres was also studied in aqueous media by removing the acetone under reduced pressure once the nanospheres are prepared. DLS measurements of the nanospheres, before and after acetone removal, confirmed their stability in aqueous media up to 100 h (See SI, Figure S118 and S119).

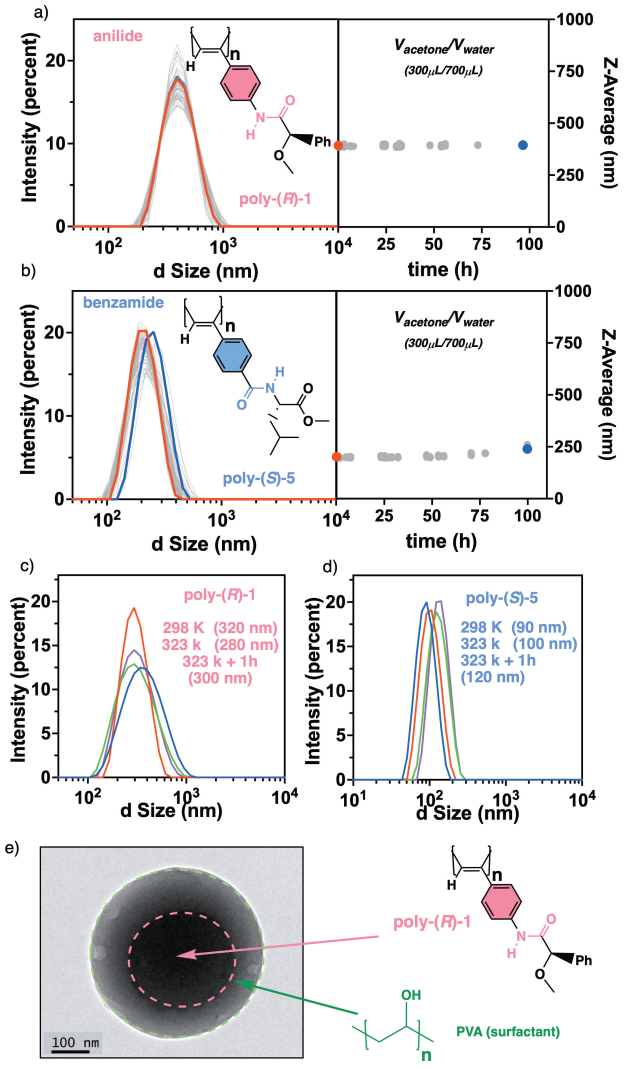

Figure 6. DLS studies of (a,c) anilide—poly-(*R*)-**1**—and (b,d) benzamide—poly-(*S*)-**5**—over time in acetone/water 300/700 ratio and after thermal treatment. e) TEM image of poly-(*R*)-**1** nanospheres stabilized with PVA.

The thermal stability of the polymer particles was also tested by heating the dispersions of poly-(*R*)-**1** and poly-(*S*)-**5** up to 323 K. DLS experiments demonstrated that the particles remain stable after heating the dispersions to 323 K for 1 h (Figures 6c–d).

In addition to these stability studies in the absence of surfactant, the nanosphere surface was decorated with a surfactant such as poly(vinylalcohol) (PVA). For this purpose, different amount of PVA were added to prepared dispersions of 0.3 mg of poly-(*R*)-**1** in 300μL/700μL acetone/water mixture until reach PPA (m.r.u.)/PVA (m.r.u.) ratios of 1.0/0.2, 1.0/0.4, 1.0/0.6, 1.0/1.0 (equiv/equiv). DLS studies before and after the addition of PVA showed an increase in the polymer particle size, which increases when the amount of PVA also increases (see Figure 6e and SI). TEM images of poly-(*R*)-**1**/PVA particles show how PVA coats the poly-(*R*)-**1** nanospheres, generating an outer layer whose thickness depends on the amount of PVA added (Figure 6e).

Polymer particle encapsulation and UV/Vis light-triggered release studies. The encapsulation ability of these chiral polymer particles was explored by selecting, as guest, fluorescent dyes (5,6-carboxyfluorescein, rhodamine B isothiocyanate) and fluorescent particles (quantum dots). Thus, nanospheres of poly-(*R*)-**1** with diameter ca. 400 nm were prepared in a 500/500 (μL/μL) acetone/water mixture in the presence of these dyes or fluorescent particles. Confocal microscopy studies show nanospheres with different emission colors depending on the dye encapsulated, e.g. a bright green emission for nanospheres containing 5,6-carboxyfluorescein and a red-orange color emission for those containing quantum dots or rhodamine (Figures 7a–c).

From literature, it is known that poly(phenylacetylene)s are light-sensitive due to a photochemical electrocyclization of the polyene backbone under light exposure (Figure 7d).[14,28] The rate of this photochemical electrocyclization of PPAs is directly related to the secondary structure of the PPA (ω_1), being faster for compressed than for stretched helices. Therefore, as a proof of concept, we wanted to explore the release of encapsulated substances by irradiating a dispersion of polymer particles with UV/Vis light.

Thus, we analyzed first the photostability of poly-(*R*)-**2** in the macromolecularly dissolved (acetone) and in the aggregated [acetone/water 500/500 (μL/μL)] states ([poly-(*R*)-**2**] = 0.3 mg/mL). Interestingly, nanostructuration of poly-(*R*)-**2** led to an increase in the photostability of the PPA, such that the half time needed to photoisomerize the polyene backbone increases from 12 to 37 minutes (Figure S120). Similar experiments were carried out for poly-(*S*)-**5**, again observing that photostability increases in the aggregated state (10 min) with respect to the macromolecu-

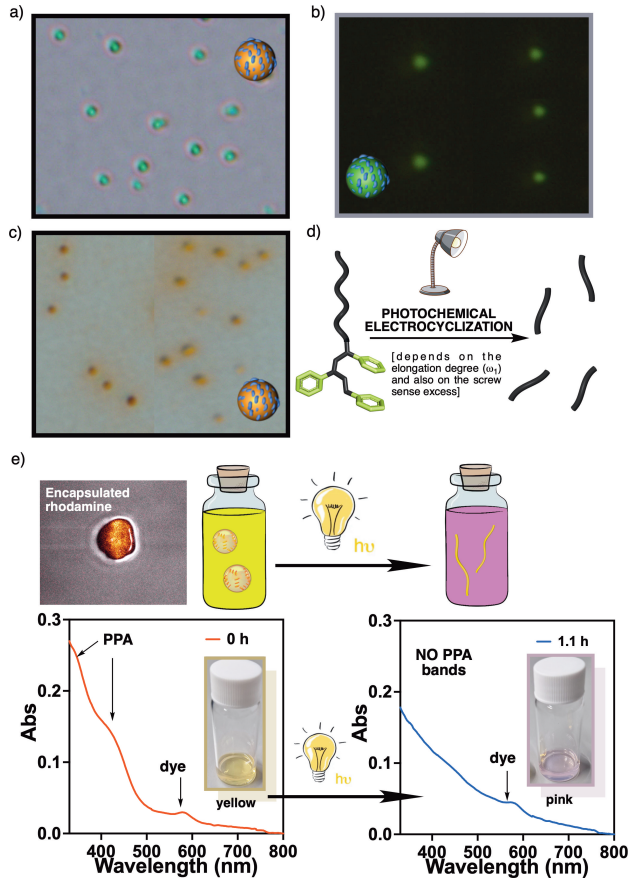

Figure 7. Confocal images of poly-(*R*)-**1** polymer particles prepared in a 500/500 (μL/μL) acetone/water mixture in the presence of (a) quantum dots, (b) 5,6-carboxyfluorescein and (c) rhodamine B isothiocyanate. d) Illustration of the photochemical electrocyclization of a PPA under UV/Vis light. e) Solution colour and UV/Vis studies of poly-(*R*)-**2** encapsulating rhodamine B isothiocyanate before and after light irradiation.

larly dissolved state (8 min) (Figure S121). The difference in the photoisomerization rates of poly-(*R*)-**2** and poly-(*S*)-**5** lies in the adoption of different scaffolds (ω_1, ca. 148° for poly-(*S*)-**5** and ca. 155° for poly-(*R*)-**2**) with different screw sense excesses. An analogous experiment was then carried out for a dispersion of poly-(*R*)-**2** prepared in acetone/water 500/500 (μL/μL) and in the presence of rhodamine B isothiocyanate. Before light irradiation, confocal images revealed the existence of nanospheres that had trapped the dye inside. Moreover, UV/Vis spectra showed the presence of polymer particles that encapsulated the dye, resulting in a yellowish solution (Figures 7e and S122). After 1.1 h of light irradiation, the polymer particles were immolated by photochemical electrocyclization of the polyene backbones, releasing rhodamine B isothiocyanate and changing the color of the solution from yellow to pink.

Conclusion

In this work, we have demonstrated by using a library of PPAs [poly-(**1**–**9**)] that nanoprecipitation in the absence of surfactants at different acetone/water or THF/water ratios can be a useful and robust methodology to generate stable chiral polymer particles with tunable size. The only requirement observed during these studies is the use of PPAs with a non-stretched helical scaffold ($\omega_1 < 165°$). Interestingly, these studies also showed that variations in the acidic behavior of the amide bond used to connect the pendant to the PPA backbone can affect the density of the polymer particle, without altering the size or morphology of the aggregates. Thus, anilide-PPAs, containing a more acidic amide group, produce dense nanospheres probably due to the formation of many strong hydrogen bonds between polymer chains. On the other hand, benzamide-PPAs, containing less acidic amide groups, generate fluffier nanospheres, probably due to the formation of fewer and weaker hydrogen bonding interactions between polymer chains.

For those PPAs adopting a highly stretched and almost planar macromolecular structure ($\omega_1 > 165°$), it is not possible to control their aggregation via nanoprecipitation. These polymers have a hydrophobic polyphenylacetylene core exposed to the solvent. As a result, in the presence of water, these polymers have a high tendency to aggregate, making not possible to control the size or shape of the aggregates.

The polymer particles prepared by nanoprecipitation of PPAs with $\omega_1 < 165°$ have shown good temporal (up to 100 h) and thermal (up to 323 K) stabilities. Moreover, these polymer particles can encapsulate different molecules or particles such as fluorescent dyes or quantum dots. The release of the encapsulated material can be accomplished by light irradiation, which destroys the polymer particle by photochemical electrocyclization of the polyene backbone. The rate of this photochemical process depends on the ω_1 dihedral angle and the screw sense excess adopted by the PPA.

The generation of these "tailor-made" chiral polymer particles, which combine the capability to encapsulate different types of materials and a dynamic chiral surface, opens the door to the creation of supramolecular assemblies with controlled size and tunable chiral cores and surfaces. The relationship between PPA secondary structure (ω_1 and screw sense excess) and photochemical electrocyclization allows us to consider the possibility of controlling the release rate of encapsulated substances, which can be of great interest in medicinal, biological, or material sciences, as well as to study encapsulation and delivery processes.

Supporting Information

Chemical structure of monomers and polymers, materials and methods, synthesis and characterization of monomers, oligomers and polymers, spectroscopy studies, nanostructuration of polymers, microscopy studies, dynamic light scattering experiments, stability studies.

The Supporting Information is available free of charge on the ACS Publications website.

Acknowledgements

Financial support from AEI (PID2022-136848NB-I00), Xunta de Galicia (ED431C 2022/21, Centro Singular de Investigación de Galicia acreditación 2023–2027, ED431G 2023/03, and the European Regional Development Fund (ERDF) and is gratefully acknowledged. M. N.-M. and M. F.-M. thanks MICINN for FPI contracts. We also thank Servicio de Microscopía Electrónica (RIAIDT, Universidad de Santiago de Compostela) for SEM and TEM studies.

Conflict of Interest

The authors declare no conflict of interest.

Data Availability Statement

The data that support the findings of this study are available in the supplementary material of this article.

Keywords: nanospheres · helical polymers · encapsulation · poly(phenylacetylene)s · secondary structure

[1] K. S. Park, Z. Xue, B. Patel, H. An, J. J. Kwok, P. Kafle, Q. Chen, D. Shukla, Y. Diao, *Nat. Commun.* **2022**, *13*, 2738.
[2] L. Xu, M. Guo, C. Hung, X.-L. Shi, Y. Yuan, X. Zhang, R.-H. Jin, W. Li, Q. Dong, D. Zhao, *J. Am. Chem. Soc.* **2023**, *145*(14), 7810–7819.
[3] D. Medina, Y. Mastai, *Isr. J. Chem.* **2018**, *58*, 1330–1337.
[4] H. Zhong, J. Deng, *Polym. Rev.* **2022**, *62*, 826–859.
[5] H. Zhong, B. Zhao, J. Deng, *Small* **2023**, 2300961.
[6] F. Freire, E. Quiñoá, R. Riguera, *Chem. Rev.* **2016**, *116*, 1242–1271.
[7] L. R. MacFarlane, H. Shaikh, J. D. Garcia-Hernandez, M. Vespa, T. Fukui, I. Manners, *Nat. Rev. Mater.* **2021**, *6*, 7–26.
[8] H. Zhong, H. Yang, J. Shang, B. Zhao, J. Deng, *Nanoscale* **2022**, *14*, 16893–16901.
[9] G. Zhang, X. Cheng, Y. Wang, W. Zhang, *Aggregate* **2023**, *4*, e262.
[10] E. Yashima, K. Maeda, H. Lida, Y. Furusho, K. Nagai, *Chem. Rev.* **2009**, *109*, 6102–6211.
[11] E. Yashima, K. Maeda, *Macromolecules* **2008**, *41*, 3–12.
[12] B. M. Rosen, C. J. Wilson, D. A. Wilson, M. Peterca, M. R. Imam, V. Percec, *Chem. Rev.* **2009**, *109*, 6275–6540.
[13] E. Suárez-Picado, E. Quiñoá, R. Riguera, F. Freire, *Chem. Mater.* **2018**, *30*, 6908–6914.
[14] F. Rey-Tarrío, R. Rodríguez, E. Quiñoá, R. Riguera, F. Freire, *Angew. Chem. Int. Ed.* **2021**, *60*, 8095–8103.
[15] T. Ikai, T. Kurake, S. Okuda, K. Maeda, E. Yashima, *Angew. Chem. Int. Ed.* **2021**, *60*, 4625–4632.
[16] R. Rodríguez, E. Suárez-Picado, E. Quiñoá, R. Riguera, F. Freire, *Angew. Chem. Int. Ed.* **2020**, *59*, 8616–8622.
[17] E. Yashima, N. Ousaka, D. Taura, K. Shimomura, T. Ikai, K. Maeda, *Chem. Rev.* **2016**, *116*, 13752–13990.
[18] T. Nakano, Y. Okamoto, *Chem. Rev.* **2001**, *101*, 4013–4038.
[19] E. Schwartz, M. Koepf, H. Kitto, R. J. M. Nolte, A. E. Rowan, *Polym. Chem.* **2011**, *2*, 33–47.
[20] K. Maeda, M. Nozaki, K. Hashimoto, K. Shimomura, D. Hirose, T. Nishimura, G. Watanabe, E. Yashima, *J. Am. Chem. Soc.* **2020**, *142*, 7668–7682.
[21] M. Núñez-Martínez, E. Quiñoá, F. Freire, *Nanoscale* **2022**, *14*, 13066–13072.
[22] E. Yashima, K. Maeda, Y. Furusho, *Acc. Chem. Res.* **2008**, *41*, 1166–1180.
[23] R. Ishidate, A. J. Markvoort, K. Maeda, E. Yashima, *J. Am. Chem. Soc.* **2019**, *141*, 7605–7614.
[24] M. Nuñez-Martínez, S. Arias, E. Quiñoá, R. Riguera, F. Freire, *Chem. Mater.* **2021**, *33*, 4805–4812.
[25] R. Rodríguez, E. Quiñoá, R. Riguera, F. Freire, *J. Am. Chem. Soc.* **2016**, *138*, 9260–9628.
[26] S. Leiras, E. Suárez-Picado, E. Quiñoá, R. Riguera, F. Freire, *Giant* **2020**, *7*, 100068.
[27] M. Lago, M. Cid, E. Quiñoá, F. Freire, *Angew. Chem. Int. Ed.* **2023**, *62*, e2023003329.
[28] F. Rey-Tarrío, R. Rodríguez, E. Quiñoá, F. Freire, *Nat. Commun.* **2023**, *17*, 1742.
[29] F. Rey-Tarrío, S. Guisán-Ceinós, J. Cuerva, D. Miguel, M. Ribagorda, E. Quiñoá, F. Freire, *Angew. Chem. Int.* **2022**, *61*, e202207623.
[30] M. Núñez-Martínez, S. Arias, J. Bergueiro, E. Quiñoá, R. Riguera, F. Freire, *Macromol. Rapid Commun.* **2022**, *43*, 2100616.
[31] E. Suárez-Picado, E. Quiñoá, R. Riguera, F. Freire, *Angew. Chem. Int. Ed.* **2020**, *59*, 4537–4543.
[32] M. Núñez-Martínez, E. Quiñoá, F. Freire, *Chem. Mater.* **2023**, *35*, 4865–4872.
[33] S.-Y. Li, L. Xu, R.-T. Gao, Z. Cheng, N. Liu, Z.-Q. Wu, *J. Mater. Chem. C* **2023**, *11*, 1242–1250.
[34] N. Liu, R.-T. Gao, Z.-Q. Wu, *Acc. Chem. Res.* **2023**, *56*, 2954–2967.
[35] L. Zhou, C.-L. Li, R.-T. Gao, S.-M. Kang, L. Xu, X.-H. Xu, N. Liu, Z.-Q. Wu, *Macromolecules* **2021**, *54*, 679–686.
[36] Z.-Q. Wu, X. Song, Y.-X. Li, L. Zhou, Y.-Y. Zhu, Z. Chen, N. Liu, *Nat. Commun.* **2023**, *14*, 566.
[37] M. Lago-Silva, M. Fernández-Míguez, R. Rodríguez, E. Quiñoá, F. Freire, *Chem. Soc. Rev.* **2024**, *53*, 793–852.
[38] Z. Tang, H. Iida, H.-Y. Hu, E. Yashima, *ACS Macro Lett.* **2012**, *1*, 261–265.
[39] L. Liu, Y. Wang, F. Wang, C. Zhang, Y. Zhou, Z. Zhou, X. Liu, R. Zhu, H. Dong, T. Satoh, *React. Funct. Polym.* **2020**, *146*, 104392.
[40] X.-H. Xu, S.-M. Kang, R.-T. Gao, Z. Chen, N. Liu, Z.-Q. Wu, *Angew. Chem. Int. Ed.* **2023**, *62*, e202300882.
[41] L. Xu, Y.-J. Wu, R.-T. Gao, S.-Y. Li, N. Liu, Z.-Q. Wu, *Angew. Chem. Int. Ed.* **2023**, *62*, e202217234.
[42] S. Wang, D. Hu, X. Guan, S. Cai, G. Shi, Z. Shuai, J. Zhang, Q. Peng, X. Wan, *Angew. Chem. Int. Ed.* **2021**, *60*, 21918–21926.
[43] D. Hirose, A. Isobe, E. Quiñoá, F. Freire, K. Maeda, *J. Am. Chem. Soc.* **2019**, *141*, 8592–8598.
[44] Y. Zhao, X. Zhang, W. Li, A. Zhang, *Eur. Polym. J.* **2019**, *118*, 275–279.
[45] D. Zhang, C. Song, J. Deng, W. Yang, *Macromolecules* **2012**, *45*, 7329–7338.
[46] B. Chen, C. Song, X. Luo, J. Deng, W. Yang, *Macromol. Rapid Commun.* **2011**, *32*, 1986–1992.
[47] Y. Yang, N. Bajaj, P. Xu, K. Ohn, M. D. Tsifansky, Y. Yeo, *Biomaterials* **2009**, *30*, 1947–1953.
[48] Y. Zhang, J. Deng, K. Pan, *Macromolecules* **2018**, *51*, 8878–8886.
[49] X. Yong, Y. Wu, J. Deng, *Polym. Chem.* **2019**, *10*, 4441–4448.

[50] L. Yin, H. Duan, T. Chen, D. Qi, J. Deng, *Polym. Chem.* **2021**, *12*, 6404–6416.
[51] F. Freire, J. M. Seco, E. Quiñoá, R. Riguera, *J. Am. Chem. Soc.* **2012**, *134*, 19374–19383.
[52] J. Bergueiro, M. Núñez-Martínez, S. Arias, E. Quiñoá, R. Riguera, F. Freire, *Nanoscale Horiz.* **2020**, *5*, 495–500.
[53] S. Arias, M. Núñez-Martínez, E. Quiñoá, R. Riguera, F. Freire, *Polym. Chem.* **2017**, *8*, 3740–3745.
[54] S. Arias, M. Núñez-Martínez, E. Quiñoá, R. Riguera, F. Freire, *Small* **2017**, *13*, 1602398..
[55] R. Rodríguez, S. Arias, E. Quiñoá, R. Riguera, F. Freire, *Nanoscale* **2017**, *9*, 17752–17757.
[56] S. Arias, F. Freire, E. Quiñoá, R. Riguera, *Angew. Chem. Int. Ed.* **2014**, *53*, 13720–13724.
[57] S. Leiras, F. Freire, J. M. Seco, E. Quiñoá, R. Riguera, *Chem. Sci.* **2013**, *4*, 2735–2743.
[58] T. Taniguchi, T. Yoshida, K. Echizen, K. Takayama, T. Nishimura, K. Maeda, *Angew. Chem. Int. Ed.* **2020**, *59*, 8670–8680.
[59] S. Sakamoto, T. Taniguchi, Y. Sakata, S. Akine, T. Nishimura, K. Maeda, *Angew. Chem. Int. Ed.* **2021**, *60*, 22201–22206.
[60] K. Echizen, T. Taniguchi, T. Nishimura, K. Maeda, *J. Am. Chem. Soc.* **2021**, *143*, 3604–3612.
[61] S. Mishra, A. K. Mondal, E. Z. B. Smolinsky, R. Naaman, K. Maeda, T. Nishimura, T. Taniguchi, T. Yoshida, K. Takayama, E. Yashima, *Angew. Chem. Int. Ed.* **2020**, *59*, 14671–14676.

Manuscript received: February 16, 2024
Accepted manuscript online: May 14, 2024
Version of record online: July 9, 2024